B.1.1.529 escapes the majority of SARS-CoV-2 neutralizing antibodies of diverse epitopes

Yunlong Cao[1,2,#,*], Jing Wang[1,3,#], Fanchong Jian[1,4,#], Tianhe Xiao[1,5,#], Weiliang Song[1,3,#], Ayijiang Yisimayi[1,3,#], Weijin Huang[6,#], Qianqian Li[6], Peng Wang[1], Ran An[1], Jing Wang[1], Yao Wang[1], Xiao Niu[1,4], Sijie Yang[1,7], Hui Liang[1], Haiyan Sun[1], Tao Li[6], Yuanling Yu[6], Qianqian Cui[6], Shuo Liu[6], Xiaodong Yang[8], Shuo Du[3], Zhiying Zhang[3], Xiaohua Hao[9], Fei Shao[1], Ronghua Jin[9], Xiangxi Wang[10,*], Junyu Xiao[2,3,*], Youchun Wang[6,*], Xiaoliang Sunney Xie[1,2,*]

[1]Biomedical Pioneering Innovation Center (BIOPIC), Peking University, Beijing, P.R. China.
[2]Beijing Advanced Innovation Center for Genomics (ICG), Peking University, Beijing, P.R. China.
[3]School of Life Sciences, Peking University, Beijing, P.R. China.
[4]College of Chemistry and Molecular Engineering, Peking University, Beijing, P.R. China.
[5]Joint Graduate Program of Peking-Tsinghua-NIBS, Academy for Advanced Interdisciplinary Studies, Peking University, Beijing, China.
[6]Division of HIV/AIDS and Sex-transmitted Virus Vaccines, Institute for Biological Product Control, National Institutes for Food and Drug Control (NIFDC), and WHO Collaborating Center for Standardization and Evaluation of Biologicals, Beijing, P.R. China.
[7]Tsinghua-Peking Center for Life Sciences, Beijing, P.R. China.
[8]Beijing YouAn Hospital, Capital Medical University, Beijing, P.R. China.
[9]Beijing Ditan Hospital, Capital Medical University, Beijing, P.R. China.
[10]CAS Key Laboratory of Infection and Immunity, National Laboratory of Macromolecules, Institute of Biophysics, Chinese Academy of Sciences, Beijing, P.R. China.
[*]Correspondence: Yunlong Cao (yunlongcao@pku.edu.cn); Junyu Xiao (junyuxiao@pku.edu.cn); Xiangxi Wang (xiangxi@ibp.ac.cn); Youchun Wang (wangyc@nifdc.org.cn); Xiaoliang Sunney Xie (sunneyxie@biopic.pku.edu.cn)
[#]These authors contributed equally.

Abstract

The SARS-CoV-2 B.1.1.529 variant (Omicron) contains 15 mutations on the receptor-binding domain (RBD). How Omicron would evade RBD neutralizing antibodies (NAbs) and humoral immunity requires immediate investigation. Here, we used high-throughput yeast display screening[1,2] to determine the RBD escaping mutation profiles for 247 human anti-RBD NAbs identified from SARS-CoV/SARS-CoV-2 convalescents and vaccinees. Based on the results, NAbs could be unsupervised clustered into six epitope groups (A-F), which is highly concordant with knowledge-based structural classifications[3-5]. Strikingly, various single mutations of Omicron could impair NAbs of different epitope groups. Specifically, NAbs in Group A-D, whose epitope overlaps with ACE2-binding motif, are largely escaped by K417N, N440K, G446S, E484A, Q493K, and G496S. Group E (S309 site)[6] and F (CR3022 site)[7] NAbs, which often exhibit broad sarbecovirus neutralizing activity, are less affected by Omicron, but still, a subset of NAbs are escaped by G339D, S371L, and S375F. Furthermore, B.1.1.529 pseudovirus neutralization and RBD binding assay showed that single mutation tolerating NAbs could also be escaped due to multiple synergetic mutations on their epitopes. In total, over 85% of the tested NAbs are escaped by Omicron. Regarding NAb drugs, LY-CoV016/LY-CoV555 cocktail, REGN-CoV2 cocktail, AZD1061/AZD8895 cocktail, and BRII-196 were escaped by Omicron, while VIR7831 and DXP-604 still function at reduced efficacy. Together, data suggest Omicron could cause significant humoral immune evasion, while NAbs targeting the sarbecovirus conserved region remain most effective. Our results offer instructions for developing NAb drugs and vaccines against Omicron and future variants.

Main

The SARS-CoV-2 B.1.1.529 variant was first reported to the World Health Organization (WHO) on 24 November 2021. It appears to be rapidly spreading, and the WHO classified it as a variant of concern (VOC) only two days after, designating it as Omicron [8,9]. An unusually large number of mutations are found in Omicron, including over 30 in the spike protein [10] (Fig. 1a). The receptor-binding domain, responsible for interacting with the ACE2 receptor, bears 15 of these mutations, including G339D, S371L, S373P, S375F, K417N, N440K, G446S, S477N, T478K, E484A, Q493R, G496S, Q498R, N501Y, and Y505H. Some of these mutations are very concerning due to their well-understood functional consequences, such as K417N and N501Y, which contribute to immune escape and higher infectivity [11-14]. Many other mutations' functional impacts remain to be investigated.

The S protein is the target of essentially all NAbs found in the convalescent sera or elicited by vaccines. Most of the N-terminal domain (NTD) neutralizing antibodies target an antigenic "supersite" in NTD, involving the N3 (residues 141 to 156) and N5 (residues 246 to 260) loops [15,16], and are thus very prone to NTD mutations. Omicron carries the Δ143-145 mutation, which would alter the N3 loop and most likely result in immune escape of most anti-NTD NAbs (Extended Data Fig. 1). Compared to NTD targeting NAbs, RBD targeting NAbs are particularly abundant and potent, and display diverse epitopes. Evaluating how Omicron affects the neutralization capability of anti-RBD NAbs of diverse classes and epitopes is urgently needed.

B.1.1.529 escapes NAbs of diverse epitopes

RBD-directed SARS-CoV-2 NAbs can be assigned into different classes or binding sites based on structural analyses by cryo-EM or high-resolution crystallography [3-5,17]; however, structural data only indicates the contacting amino acids, but does not infer the escaping mutations for a specific antibody. Recent advances in deep antigen mutation screening using FACS (fluorescence-activated cell sorting)-based yeast display platform has allowed

the quick mapping of all single amino acid mutations in the RBD that affect the binding of SARS-CoV-2 RBD NAbs [1,18]. The method has proven highly effective in predicting NAB drug efficacy toward mutations [2]. However, to study how human humoral immunity may react to highly mutated variants like B.1.1.529 requires mutation profiling of a large collection of NAbs targeting different regions of RBD, and FACS-based yeast display mutation screening is limited by low experimental throughput. Here we further developed a MACS (magnetic-activated cell sorting) -based screening method which increases the throughput near 100-fold and could obtain comparable data quality like FACS (Fig 1b; Extended Data Fig 2). Using this method, we quickly characterized the RBD escaping mutation profile for a total of 247 NAbs (Supplymentary Files 1-6). Half of the NAbs were part of the antibodies identified by us using single-cell VDJ sequencing of antigen-specific memory B cells from SARS-CoV-2 convalescents, SARS-CoV-2 vaccinees, and SARS-CoV convalescents who recently received SARS-CoV-2 vaccines. The other half of NAbs were identified by groups worldwide and usually have antibody-antigen structures [3,5,6,12,17,19-42] (Supplementary Files 7).

The high-throughput screening capability allowed us to classify these NAbs into six Epitope Groups (A-F) using unsupervised clustering without dependence on structural studies, and the grouping is highly concordant with the knowledge-based structural classifications [3-5,17] (Fig. 1c and 1e). In particular, Group A-D NAbs largely correspond to the RBS A-D NAbs described by Yuan et al. [4], and their epitopes include RBD residues involved in binding to ACE2. Group A and B NAbs, represented by CB6/LY-CoV016 and AZD8895 respectively, usually can only bind to the 'up' RBD, whereas most of the Group C and D members, such as LY-CoV555 and REGN10987, bind to RBDs regardless of their 'up' and 'down' conformations. Group E and F NAbs target the S309/VIR-7831 site and CR3022 site, respectively, and neutralize SARS-CoV-2 using other mechanisms than directly interfering with ACE2 binding.

Inferred from the escaping mutation profiles, various single mutations of Omicron could impair NAbs of different epitope groups (Fig 1f). Specifically, NAbs in Group A-D, whose epitope overlaps with ACE2-binding motif, are

128 largely escaped by single mutations of K417N, G446S, E484A, Q493K, and
129 G496S. Also, a subset of NAbs of Group E and are escaped by single mutations
130 of G339D, N440K, S371L, S375F. However, due to the extensive mutations
131 accumulated on Omicron's RBD, studying NAb's response to Omicron only in
132 the single mutation context is insufficient. Indeed, B.1.1.529 pseudovirus
133 neutralization and Spike ELISA binding assay showed that single mutation
134 tolerating NAbs could also be escaped by Omicron due to multiple synergetic
135 mutations on their epitopes (Fig 1d and 1f). In total, over 85% of the tested
136 human NAbs are escaped, suggesting that Omicron could cause significant
137 humoral immune evasion.
138

139 **ACE2-blocking NAbs are more vulnerable to B.1.1.529**

140 It is crucial to analyze how each group of NAbs react to Omicron to instruct the
141 development of NAb drugs and vaccines. Group A NAbs mainly contains the
142 *VH3-53/VH3-66* germline gene-encoded antibodies, which are abundantly
143 present in our current collection of SARS-CoV-2 neutralizing antibodies
144 [19,23,24,28,43-45], including several antibodies that have obtained emergency use
145 authorization (CB6/LY-CoV016) [21] or are currently being studied in clinical trials
146 (P2C-1F11/BRII-196, BD-604/DXP-604) [20,46] (Fig. 2a, e). Group A NAbs often
147 exhibit less somatic mutations and shorter CDR3 length compared to other
148 groups (Extended Data 5a, b). The epitopes of these antibodies extensively
149 overlap with the binding site of ACE2 and are often evaded by RBD mutations
150 on K417, D420, F456, A475, L455 sites (Fig 2i, Extended Data Fig 3a). Most
151 NAbs in Group A were already escaped by B.1.351 (Beta) strain, specifically
152 K417N (Extended Data Fig 7a), due to a critical salt bridge interaction between
153 Lys417 and a negatively charged residue in the antibody (Fig. 2i, m). The NAbs
154 that survived Beta strain, such as BRII-196 and DXP-604, are insensitive to the
155 K417N single site change but could also be heavily affected by the combination
156 of K417N and other RBD mutations located on their epitopes, like S477N,
157 Q493R, G496S, Q498R, N501Y, and Y505H of Omicron, causing lost or
158 reduction of neutralization (Fig 2i; Extended Data Fig 4a).
159

160 The *VH1-58* gene-encoded NAbs are enriched in Group B (Fig. 2b). These

161 NAbs such as AZD8895 [38], REGN10933 [44], and BD-836 [47] bind to the left
162 shoulder of RBD, often focusing on the far tip (Fig 2n). These NAbs are very
163 sensitive to the change of F486, N487, and G476 (Fig 2j, Extended Data Fig
164 3b). Fortunately, F486 and a few other major targeting sites of these NAbs are
165 critically involved in ACE2-binding, and therefore they are generally harder to
166 be escaped. NAbs that focus on the far tip of the left RBD shoulder, such as
167 AZD8895 and BD-836, could survive Beta (fig 2f); however, Omicron could
168 significantly reduce Group B NAbs' binding affinity to RBD, potentially through
169 S477N/T478K/E484A on their epitope (Extended Data Fig 4b) [48], resulting in
170 the loss of neutralization. Group B NAbs are mostly escaped by Omicron and
171 should not be chosen for drug development against Omicron.
172
173 Group C NAbs are frequently encoded by *VH1-2* and *VH1-69* (Fig. 2c). The
174 majority of NAbs in this group could bind to both "up" and "down" RBDs,
175 resulting in higher neutralization potency compared to other groups (Extended
176 Data Fig 5c). Several highly potent antibodies are found in Group C, including
177 BD-368-2/DXP-593 [46], C002 [3], and LY-CoV555 [49]. They bind to the right
178 shoulder of RBD (Fig 2o), and are mostly prone to the change of Glu484
179 (Extended Data Fig 3c, 4c), such as the E484K mutation found in Beta (Fig 2g).
180 The E484A mutation seen in Omicron elicited a similar escaping effect,
181 although the change to Ala is slightly subtler, and could be tolerated by certain
182 antibodies in this group (Extended Data Fig 7b). All Group C NAbs tested are
183 escaped by Omicron (Fig 2k).
184
185 Group D NAbs consist of diverse IGHV gene-encoded antibodies (Fig. 2d).
186 Prominent members in this group include REGN10987 [44] and AZD1061 [38] (Fig
187 2h). They further rotate down from the RBD right shoulder towards the S309
188 site when compared to Group C (Fig 2p). As a loop formed by residues 440-
189 449 in RBD is critical for the targeting of this group of NAbs, they are sensitive
190 to the changes of Asn440, Lys444, Gly446, and Asn448 (Extended Data Fig
191 3d, 4d). Most NAbs of Group D remain active against Beta; however, G446S
192 would substantially affect their neutralization capability against Omicron (Fig
193 2l). Also, for those NAbs that could tolerate G446S single mutation, the
194 N440K/G446S combination may significantly reduce their binding affinity,

resulting in that most Group D NAbs are escaped by Omicron.

SARS cross-reactive NAbs are less affected by B.1.1.529

Group E and F NAbs are rarer when compared to the other four groups. The archetypical member of each group was originally isolated from a SARS-CoV convalescent, and displays SARS-CoV-2 cross-neutralizing activity. There is no clear VDJ convergent effect compared to Group A, B, and C (Fig 3a, b), and the mutation rate and CDR3 length are larger than other groups. NAbs in Group E and F rarely compete with ACE2; thus, their average IC50 is higher than NAbs in Group A-D (Extended Data 5c, d, e). High-resolution structures of Group E and F NAbs are limited; thus, their epitope distribution and neutralization mechanism are not well-understood.

NAbs in Group E, such as VIR7831/S309, may recognize a mixed protein/carbohydrate epitope, involving the N-linked glycan on Asn343 [6]. Inferred from the escaping mutation profiles (Fig 3c), Group E NAbs are often sensitive to changes of R346, T345, and G339 (Extended Data Fig 3e, 4e). The G339D mutation would affect a subset of NAbs' neutralization performance. Also, part of Group E NAbs' epitope would extend to the 440-449 loop, making them sensitive to N440K and G446S on Omicron (Fig 3e).

Group F NAbs such as CR3022 and S304 target a cryptic site in RBD that is generally not exposed (Fig 3h, i), therefore their neutralizing activities are generally weaker [7]. Group F NAbs are often sensitive to changes of K378, T376, and F374 (Extended Data Fig 3f, 4f). A loop involving RBD residues 371-375 lies in the ridge between the E and F sites; therefore, a subset of Group F NAbs, including some Group E NAbs, could be affected by the S371L/S373P/S375F mutations if their epitopes extend to this region (Fig 3d, f). Interestingly, a part of Group F NAbs is highly sensitive to G504 and V503, similar to the epitopes of S2. (Fig 3j), suggesting that they can compete with ACE2. Indeed, several NAbs, such as BD55-5300 and BD55-3372, exhibited high neutralization potency compared to other NAbs in Group F. However, These antibodies' neutralization capability might be undermined by N501Y and

229 Y505H of Omicron.

230

231 **B.1.1.529 escapes the majority of NAb drugs**

232

233 As for NAb drugs, consistent with their escaping mutation profiles, LY-
234 CoV016/LY-CoV555 cocktail, REGN-10933/REGN-109876 cocktail, and
235 AZD1061 are escaped by Omicron (Fig 4a). The binding affinity of AZD8895
236 and BRII-196 toward Omicron RBD is significantly reduced, potently due to
237 multiple mutations accumulating on their epitopes, such that AZD8895 and
238 BRII-196 failed to neutralize Omicron. VIR7831 retains strong RBD binding
239 capability, although Gly339 is part of its epitope, the G339D mutation in
240 Omicron does not appear to affect VIR7831's binding; however, VIR7831's
241 IC50 is slightly reduced to 181 ng/mL. DXP-604's binding affinity against
242 Omicron RBD is largely reduced compared to wildtype RBD; nevertheless, it
243 can still neutralize Omincron at an IC50 of 280 ng/mL, a nearly 30-fold reduction
244 compared to wildtype (Fig 4b). Additionally, several NAbs in Group E and F
245 have shown high potency against Omicron and broad pan-sarbecovirus
246 neutralization ability, promising for NAb drug development (Fig 4c). Many more
247 NAbs identified from vaccinated SARS convalescents are waiting to be
248 characterized.

249

250 **Discussion**

251

252 The high-throughput yeast screening method provides a laboratory means for
253 quickly examining the evolution outcome under a particular NAb, however, the
254 current throughput using FACS is limited and can't be used to evaluate a large
255 NAb library. By virtue of MACS, we are able to increase the throughput by two
256 orders of magnitude. In doing so, we were able to gain statistical confidence for
257 the survival proportion of anti-RBD NAbs in each epitope group against
258 Omicron. In addition to mutations in the RBD, changes in other regions of the
259 S protein are also concerning. The Δ69-70 mutation in the N-terminal domain
260 (NTD) may enhance viral infectivity [50]. The P681H mutation, located in the furin
261 cleavage site, could promote furin cleavage and therefore accelerate cell

262 fusion, similar to P681R [51].
263
264 To date, a large number of SARS-CoV-2 NAbs have been identified from
265 convalescents and vaccinees. The most potent NAbs are frequently found in
266 Groups A-D as we described above, and tend to directly interfere with the
267 binding of ACE2. Nevertheless, the neutralizing powers of these NAbs are often
268 abrogated by RBD mutations in the evolutionary arms race between SARS-
269 CoV-2 and human humoral immunity. Indeed, we showed that Omicron would
270 escape from the majority of SARS-CoV-2 NAbs in this collection. Some
271 superpotent NAbs in Group A may still function due to their extremely high
272 affinity for RBD (such as DXP604), albeit at reduced efficacy. A subset of Group
273 B NAbs (including AZD8895) is also more difficult to be evaded by single amino
274 acid changes, as they target a small epitope involving several RBD residues
275 that are essential for ACE2 binding; however, Omicron significantly reduced the
276 binding affinity of those NAbs, possibly through multiple synergetic mutations,
277 eventually causing lost of neutralization. On the other hand, Groups E and F
278 NAbs are less affected by Omicron, likely because they are not abundant in
279 population, hence exerting less evolutionary pressure for RBD to mutate in the
280 corresponding epitope groups. These NAbs target conserved RBD regions in
281 Sarbecovirus and therefore are ideal targets for future development of pan-
282 Sarbecovirus NAb drugs.
283
284 Our study also offers important instructions for vaccine design. Vaccines are
285 the most important tools for eventually vanquishing the SARS-CoV-2
286 pandemic. Based on our findings, we hypothesize that a vaccination strategy
287 that helps to enrich Groups E and F NAbs would be promising to achieve broad
288 protection. Along this line, Tan et al. recently showed that high-level and broad-
289 spectrum NAbs are present in the SARS-CoV convalescents who have
290 received an mRNA vaccine based on the SARS-CoV-2 Spike [52]. We suspect
291 that Groups E and F NAbs existed in SARS-CoV convalescents and might have
292 been boosted upon SARS-CoV-2 vaccination. Because Groups E and F NAbs
293 are the only effective NAbs against Omicron, the vaccines preferentially
294 stimulating these antibodies are highly desired. Future studies are required to
295 investigate a potential serial immunization scheme involving different

inactivated Sarbecoviruses or their RBDs is capable of broadly protecting from future SARS-CoV-2 VOCs and even future Sarbecoviruses.

Acknowledgments

We thank Professor Jesse Bloom for his generous gift of the yeast SARS-CoV-2 RBD libraries. We thank Beijing BerryGenomics for the help on DNA sequencing. We thank Sino Biological Inc. for the technical assistance on mAbs and B.1.1.529 RBD expression. This project is financially supported by the Ministry of Science and Technology of China (CPL-1233).

Author contributions

Y.C. and X.S.X designed the study. Y.C. and F.S coordinated the characterizations of the NAbs. J.W., F.J., H.L., H.S. performed and analyzed the yeast display mutation screening experiments. T.X., W.J., X.Y., P.W., H.L. performed the pseudovirus neutralization assays. W.H., Q.L., T.L., Y.Y., Q.C., S.L., Y.W. prepared the VSV-based SARS-CoV-2 pseudovirus. A.Y., Y.W., S.Y., R.A., W.S. performed and analyzed the antigen-specific single B cell VDJ sequencing. X.N., R.A. performed the antibody BLI studies. Z.C., S.D., P.L., L.W., Z.Z., X.W., J.X. performed the antibody structural analyses. P.W., Y.W., J.W, H.S, H.L. performed ELISA experiment. X.H. and R.J. coordinated the blood samples of vaccinated SARS convalescents. Y.C., X.W., J.X., X.S.X wrote the manuscript with inputs from all authors.

Declaration of interests

X.S.X. and Y.C. are inventors on the patent application of DXP-604 and BD series antibodies. X.S.X. and Y.C. are founders of Singlomics Biopharmaceuticals Inc. Other authors declare no competing interests.

Methods

Antigen-specific B cell sorting and sequencing

PBMCs were separated from whole blood samples based on the detailed protocol as described previously [12]. Briefly, blood samples were first diluted with 2% FBS (Gibco) in PBS (Invitrogen) and subjected to Ficoll (Cytiva) gradient

330 centrifugation. After red blood cell lysis and washing steps, PBMCs were
331 resuspended with 2% FBS in PBS for downstream B cell isolation or 10%
332 DMSO (Sigma-Aldrich) in FBS for further preservation.
333 Starting with freshly isolated or thawed PBMCs, B cells were enriched by
334 positive selection using a CD19+ B cell isolation kit according to the
335 manufacturer's instructions (STEMCELL). The enriched B cells were stained in
336 FACS buffer (1× PBS, 2% FBS, 1 mM EDTA) with the following anti-human
337 antibodies and antigens: FITC anti-CD19 Antibody (Biolegend), FITC anti-
338 CD20 Antibody (Biolegend), Brilliant Violet 421 anti-CD27 Antibody
339 (Biolegend), PE/Cyanine7 anti-IgM, and fluorophore-labelled RBD (SARS-
340 CoV-2 and SARS-CoV RBD, Sino Biological Inc.) and ovalbumin (Ova) for 30
341 min on ice. Cells were stained with 7-AAD for 10 minutes before sorting. Single
342 CD19 or CD20+ CD27+ IgM- Ova- RBD-PE+ RBD-APC+B cells were sorted
343 on an Astrios EQ (BeckMan Coulter) into PBS containing 30% FBS. Cells
344 obtained after FACS were proceed to 5′-mRNA and V(D)J libraries preparation
345 as previously described[12], which were further submitted to illumine sequencing
346 on a Hiseq 2500 platform, with the 26x91 pair-end reading mode.
347

348 **V(D)J sequence data analysis**

349 The raw FASTQ files were processed by Cell Ranger (version 6.1.1) pipeline
350 using GRCh38 reference. Sequences were generated using "cellranger multi"
351 or "cellranger vdj" with default parameters. Then we extracted the protein
352 sequences and processed them by IMGT/DomainGapAlign (version 4.10.2) to
353 obtain the annotations of V(D)J, regions of CDR and the mutation
354 frequency[53,54]. Mutation count divided by the length of V gene peptide is defined
355 as the amino acid mutation rate of V gene.
356

357 **Recombinant antibody production**

358 Paired immunoglobulin heavy and light chain genes obtained from 10X
359 Genomics V(D)J sequencing and analysis were submitted to recombinant
360 monoclonal antibody synthesis. Briefly, heavy and light genes were cloned into
361 expression vectors respectively based on Gibson assembly, which were

362 subsequently co-transfected into HEK293 cells. Then secreted monoclonal
363 antibodies from cultured cell were purified by protein A affinity chromatography.
364 The specificities of these antibodies were determined by ELISA binding
365 analysis.
366

367 **ELISA and neutralization assay**

368 ELISA were conducted to evaluate antibody or plasma binding ability. Briefly,
369 after coating with 0.03 μg/mL and 1 μg/mL RBD (Sino Biological Inc.) of different
370 sarbecovirus and SARS-CoV-2 variants, blocking, and washing, 1μg/mL
371 antibodies or serially diluted plasma samples were added to the plates. After
372 incubation and wash, plates were incubated with diluted goat anti-human IgG
373 (H+L)/HRP (JACKSON). Then plates were developed by addition of the TMB
374 (Solarbio), then the developing reaction was stopped by adding H_2SO_4 and
375 OD450 was measured by a ELISA microplate reader.
376 Neutralization assay was performed to evaluate neutralizing ability of antibody
377 and plasma the detailed process was previously described by Cao et al.[12].
378 Briefly, serially diluted antibodies were first incubated with pseudotyped virus
379 for 1h, and the mixture was then incubated with Huh-7 cells. After 24h
380 incubation in an incubator at 37℃, cells were collected and lysed with luciferase
381 substrate (PerkinElmer), then proceed to luminescence intensity measurement
382 by a microplate reader. IC50 and NT50 were determined by a four-parameter
383 non-linear regression model. Omicron pseudovirus contains the following
384 mutations: A67V, H69del, V70del, T95I, G142D, V143del, Y144del, Y145del,
385 N211del, L212I, ins214EPE, G339D, S371L, S373P, S375F, K417N, N440K,
386 G446S, S477N, T478K, E484A, Q493R, G496S, Q498R, N501Y, Y505H,
387 T547K, D614G, H655Y, N679K, P681H, N764K, D796Y, N856K, Q954H,
388 N969K, L981F.
389

390 **Biolayer interferometry**

391 Biolayer interferometry assays were conducted on Octet® R8 Protein Analysis
392 System (Fortebio) following the manufacturer's instruction. Briefly, after
393 baseline calibration, Protein A biosensors (Fortebio) were immersed with
394 antibodies to capture the antibody, then sensors were immersed in PBS with

395 0.05% Tween-20 to the baseline. After association with different concentrations
396 of RBD or Spike of Sarbecovirus and SARS-CoV-2 variants (Omicron RBD:
397 40592-V08H85, Omicron Spike: 40589-V08H26), disassociation was
398 conducted. Data were recorded using software Data Acquisition 11.1 (Fortebio)
399 and analyzed using software Data Analysis HT 11.1 (Fortebio).
400

401 **RBD Deep Mutational Scanning Library construction**

402 The yeast-display RBD mutant libraries used here were constructed as
403 described by Starr et al.,[13] based on the spike receptor binding domain (RBD)
404 from SARS-CoV-2 (NCBI GenBank: MN908947, residues N331-T531) with the
405 modifications that instead of 16-neuclotide barcode, a unique 26-neuclotide
406 barcode was appended to each RBD variant as an identifier in order to
407 decrease sequencing cost by eliminating the use of PhiX. Briefly, three rounds
408 of mutagenesis PCR were performed with designed and synthesized
409 mutagenetic primer pools; in order to solid our conclusion, we constructed two
410 RBD mutant libraries independently. RBD mutant libraries were then cloned
411 into pETcon 2649 vector and the assembled products were electroporated into
412 electrocompetent DH10B cells to enlarge plasmid yield. Plasmid extracted form
413 E. coli were transformed into the EBY100 strain of *Saccharomyces cerevisiae*
414 via the method described by Gietz and Schiestl[55]. Transformed yeast
415 population were screened on SD-CAA selective plate and further cultured in
416 SD-CAA liquid medium at a large scale. The resulted yeast libraries were flash
417 frozen by liquid nitrogen and preserved at -80℃.
418

419 **PacBio library preparation, sequencing and analysis**

420 The correspondence of RBD gene sequence in mutant library and N26 barcode
421 was obtained by PacBio sequencing. Firstly, the bacterially-extracted plasmid
422 pools were digested by NotI restriction enzyme and purified by agarose gel
423 electrophoresis, then proceed to SMRTbell ligation. Four RBD mutant libraries
424 were sequenced in one SMRT cell on a PacBio Sequel II platform. PacBio
425 SMRT sequencing subreads were converted to HiFi ccs reads with pbccs, and
426 then processed with a slightly modified version of the script previously

427 described[13] to generate the barcode-variant dictionary. To reduce noise,
428 variants containing stop codons or supported by only one ccs read were
429 removed from the dictionary and ignored during further analysis.
430
431 **MACS-based mutation escape profiling**
432 ACE2 binding mutants were sorted based on magnetic beads to eliminate non-
433 functional RBD variants. Briefly, the biotin binder beads (Thermo Fisher) were
434 washed and prepared as the manufacturer's instruction and incubated with
435 biotinylated ACE2 protein (Sino Biological Inc.) at room temperature with mild
436 rotation. The ACE2 bound beads were washed twice and resuspend with 0.1%
437 BSA buffer (PBS supplemented with 0.1% bovine serum albumin), and ready
438 for ACE2 positive selection. Transformed yeast library were inoculated into SD-
439 CAA and grown at 30℃ with shaking for 16-18h, then back-diluted into SG-
440 CAA at 23℃ with shaking to induce RBD surface expression. Yeasts were
441 collected and washed twice with 0.1% BSA buffer and incubated with
442 aforementioned ACE2 bound beads at room temperature for 30min with mild
443 rotating. Then, the bead-bound cells were washed, resuspend with SD-CAA
444 media, and grown at 30℃ with shaking. After overnight growth, the bead-
445 unbound yeasts were separated with a magnet and cultured in a large scale.
446 The above ACE2 positive selected yeast libraries were preserved at -80℃ in
447 aliquots as a seed bank for antibody escape mapping.
448
449 One aliquot of ACE2 positive selected RBD library was thawed and inoculated
450 into SD-CAA, then grown at 30℃ with shaking for 16-18h. 120 OD units were
451 back-diluted into SG-CAA media and induced for RBD surface expression.
452 Two rounds of sequential negative selection to sort yeast cells that escape
453 Protein A conjugated antibody binding were performed according to the
454 manufacturer's protocol. Briefly, Protein A magnetic beads (Thermo Fisher)
455 were washed and resuspend in PBST (PBS with 0.02% Tween-20). Then
456 beads were incubated with neutralizing antibody and rotated at room
457 temperature for 30min. The antibody-conjugated beads were washed and
458 resuspend in PBST. Induced yeast libraries were washed and incubated with
459 antibody-conjugated beads for 30min at room temperature with agitation. The

460 supernatant was separated and proceed to a second round of negative
461 selection to ensure full depletion of antibody-binding yeast.
462
463 To eliminate yeast that did not express RBD, MYC-tag based RBD positive
464 selection was conducted according to the manufacturer's protocol. First, anti-c-
465 Myc magnetic beads (Thermo Fisher) were washed and resuspend with 1X
466 TBST, then the prepared beads were incubated for 30min with the antibody
467 escaping yeasts after two rounds of negative selection. Yeasts bound by anti-
468 c-Myc magnetic beads were wash with 1X TBST and grown overnight in SD-
469 CAA to expand yeast population prior to plasmid extraction.
470
471 Overnight cultures of MACS sorted antibody-escaped and ACE2 preselected
472 yeast populations were proceed to yeast plasmid extraction kit (Zymo
473 Research). PCRs were performed to amplify the N26 barcode sequences as
474 previously described[13]. The PCR products were purified with 0.9X Ampure XP
475 beads (Beckman Coulter) and submitted to 75bp single-end Illumina Nextseq
476 500 sequencing.
477
478 **Deep mutational scanning data processing**
479
480 Raw single-end Illumina sequencing reads were trimmed and aligned to the
481 reference barcode-variant dictionary generated as described above to get the
482 count of each variant with dms_variants Python package (version 0.8.9). For
483 libraries with N26 barcodes, we slightly modified the illuminabarcodeparser
484 class of this package to tolerate one low sequencing quality base in the barcode
485 region. The escape score of variant X is defined as F×(nX,ab / Nab) / (nX,ref /
486 Nref), where nX,ab and nX,ref is the number of detected barcodes for variant
487 X, Nab and Nref are the total number of barcodes in antibody-selected (ab)
488 library and reference (ref) library respectively as described by Starr et al. [13].
489 Different from FACS experiments, as we couldn't measure the number of cells
490 retained after MACS selection precisely, here F is considered as a scaling
491 factor to transform raw escape fraction ratios to 0-1 range, and is calculated
492 from the first and 99th percentiles of raw escape fraction ratios. Scores less
493 than the first percentile or larger than the 99th percentile are considered to be

494 outliers and set to zero or one, respectively. For each experiment, barcodes
495 detected by <6 reads in the reference library were removed to reduce the
496 impact of sampling noise, and variants with ACE2 binding below -2.35 or RBD
497 expression below -1 were removed as previously described [13]. Finally, we built
498 global epistasis models with dms_variants package for each library to estimate
499 single mutation escape scores, utilizing the Python scripts provided by Greaney
500 et al. [18].

501 **Antibody clustering**

502 Antibody clustering and epitope group identification were performed based on
503 the N×M escape score matrix, where N is the number of antibodies which pass
504 the quality controlling filters, and M is the number of informative sites on SARS-
505 CoV-2 RBD. Each entry of the matrix Anm refers to the total escape score of
506 all kinds of mutations on site m of antibody n. The dissimilarity between two
507 antibodies is defined based on the Pearson's correlation coefficient of their
508 escape score vectors, i. e. Dij=1-Corr(Ai,Aj). Sites with at least 6 escaped
509 antibodies (site escape score >1) were considered informative and selected for
510 dimensionality reduction and clustering. We utilized cmdscale R function to
511 convert the cleaned escape matrix into an N×6 feature matrix by
512 multidimensional scaling (MDS) with the dissimilarity metric described above,
513 followed by unsupervised k-medoids clustering within this 6-dimensional
514 antibody feature space. Finally, two-dimensional tSNE embeddings were
515 generated with Rtsne package for visualization.
516
517

References

1 Starr, T. N. *et al.* Prospective mapping of viral mutations that escape antibodies used to treat COVID-19. *Science* **371**, 850-854, doi:10.1126/science.abf9302 (2021).

2 Starr, T. N., Greaney, A. J., Dingens, A. S. & Bloom, J. D. Complete map of SARS-CoV-2 RBD mutations that escape the monoclonal antibody LY-CoV555 and its cocktail with LY-CoV016. *Cell Rep Med* **2**, 100255, doi:10.1016/j.xcrm.2021.100255 (2021).

3 Barnes, C. O. *et al.* SARS-CoV-2 neutralizing antibody structures inform therapeutic strategies. *Nature* **588**, 682-687, doi:10.1038/s41586-020-2852-1 (2020).

4 Yuan, M. *et al.* Structural and functional ramifications of antigenic drift in recent SARS-CoV-2 variants. *Science* **373**, 818-823, doi:10.1126/science.abh1139 (2021).

5 Dejnirattisai, W. *et al.* The antigenic anatomy of SARS-CoV-2 receptor binding domain. *Cell* **184**, 2183-2200 e2122, doi:10.1016/j.cell.2021.02.032 (2021).

6 Pinto, D. *et al.* Cross-neutralization of SARS-CoV-2 by a human monoclonal SARS-CoV antibody. *Nature* **583**, 290-295, doi:10.1038/s41586-020-2349-y (2020).

7 Yuan, M. *et al.* A highly conserved cryptic epitope in the receptor binding domains of SARS-CoV-2 and SARS-CoV. *Science* **368**, 630-633, doi:10.1126/science.abb7269 (2020).

8 Callaway, E. Heavily mutated Omicron variant puts scientists on alert. *Nature* **600**, 21, doi:10.1038/d41586-021-03552-w (2021).

9 Callaway, E. & Ledford, H. How bad is Omicron? What scientists know so far. *Nature*, doi:10.1038/d41586-021-03614-z (2021).

10 Kumar, S., Thambiraja, T. S., Karuppanan, K. & Subramaniam, G. Omicron and Delta Variant of SARS-CoV-2: A Comparative Computational Study of Spike protein. *bioRxiv* (2021).

11 Li, Q. *et al.* SARS-CoV-2 501Y.V2 variants lack higher infectivity but do have immune escape. *Cell* **184**, 2362-2371 e2369, doi:10.1016/j.cell.2021.02.042 (2021).

12 Cao, Y. *et al.* Humoral immune response to circulating SARS-CoV-2 variants elicited by inactivated and RBD-subunit vaccines. *Cell Res* **31**, 732-741, doi:10.1038/s41422-021-00514-9 (2021).

13 Starr, T. N. *et al.* Deep Mutational Scanning of SARS-CoV-2 Receptor Binding Domain Reveals Constraints on Folding and ACE2 Binding. *Cell* **182**, 1295-1310 e1220, doi:10.1016/j.cell.2020.08.012 (2020).

14 Gu, H. *et al.* Adaptation of SARS-CoV-2 in BALB/c mice for testing vaccine efficacy. *Science* **369**, 1603-1607, doi:10.1126/science.abc4730 (2020).

15 Cerutti, G. *et al.* Potent SARS-CoV-2 neutralizing antibodies directed against spike N-terminal domain target a single supersite. *Cell Host Microbe* **29**, 819-833 e817, doi:10.1016/j.chom.2021.03.005 (2021).

16 McCallum, M. *et al.* N-terminal domain antigenic mapping reveals a site of vulnerability for SARS-CoV-2. *Cell* **184**, 2332-2347 e2316, doi:10.1016/j.cell.2021.03.028 (2021).

17 Yuan, M., Liu, H., Wu, N. C. & Wilson, I. A. Recognition of the SARS-CoV-2 receptor binding domain by neutralizing antibodies. *Biochem Biophys Res Commun* **538**, 192-203, doi:10.1016/j.bbrc.2020.10.012 (2021).

18 Greaney, A. J. *et al.* Complete Mapping of Mutations to the SARS-CoV-2 Spike Receptor-Binding Domain that Escape Antibody Recognition. *Cell Host Microbe* **29**, 44-57 e49, doi:10.1016/j.chom.2020.11.007 (2021).

19 Cao, Y. *et al.* Potent Neutralizing Antibodies against SARS-CoV-2 Identified by High-Throughput Single-Cell Sequencing of Convalescent Patients' B Cells. *Cell* **182**, 73-84 e16, doi:10.1016/j.cell.2020.05.025 (2020).

20 Ju, B. *et al.* Human neutralizing antibodies elicited by SARS-CoV-2 infection. *Nature* **584**, 115-119, doi:10.1038/s41586-020-2380-z (2020).

21 Shi, R. *et al.* A human neutralizing antibody targets the receptor-binding site of SARS-CoV-2. *Nature* **584**, 120-124, doi:10.1038/s41586-020-2381-y (2020).

22 Wu, Y. *et al.* A noncompeting pair of human neutralizing antibodies block COVID-19 virus binding to its receptor ACE2. *Science* **368**, 1274-1278, doi:10.1126/science.abc2241 (2020).

23 Yuan, M. *et al.* Structural basis of a shared antibody response to SARS-CoV-2. *Science* **369**, 1119-1123, doi:10.1126/science.abd2321 (2020).

24 Robbiani, D. F. *et al.* Convergent antibody responses to SARS-CoV-2 in convalescent individuals. *Nature* **584**, 437-442, doi:10.1038/s41586-020-2456-9 (2020).
25 Liu, L. *et al.* Potent neutralizing antibodies against multiple epitopes on SARS-CoV-2 spike. *Nature* **584**, 450-456, doi:10.1038/s41586-020-2571-7 (2020).
26 Baum, A. *et al.* Antibody cocktail to SARS-CoV-2 spike protein prevents rapid mutational escape seen with individual antibodies. *Science* **369**, 1014-1018, doi:10.1126/science.abd0831 (2020).
27 Brouwer, P. J. M. *et al.* Potent neutralizing antibodies from COVID-19 patients define multiple targets of vulnerability. *Science* **369**, 643-650, doi:10.1126/science.abc5902 (2020).
28 Rogers, T. F. *et al.* Isolation of potent SARS-CoV-2 neutralizing antibodies and protection from disease in a small animal model. *Science* **369**, 956-963, doi:10.1126/science.abc7520 (2020).
29 Piccoli, L. *et al.* Mapping Neutralizing and Immunodominant Sites on the SARS-CoV-2 Spike Receptor-Binding Domain by Structure-Guided High-Resolution Serology. *Cell* **183**, 1024-1042 e1021, doi:10.1016/j.cell.2020.09.037 (2020).
30 Zost, S. J. *et al.* Potently neutralizing and protective human antibodies against SARS-CoV-2. *Nature* **584**, 443-449, doi:10.1038/s41586-020-2548-6 (2020).
31 Tortorici, M. A. *et al.* Ultrapotent human antibodies protect against SARS-CoV-2 challenge via multiple mechanisms. *Science* **370**, 950-957, doi:10.1126/science.abe3354 (2020).
32 Lv, Z. *et al.* Structural basis for neutralization of SARS-CoV-2 and SARS-CoV by a potent therapeutic antibody. *Science* **369**, 1505-1509, doi:10.1126/science.abc5881 (2020).
33 Zost, S. J. *et al.* Rapid isolation and profiling of a diverse panel of human monoclonal antibodies targeting the SARS-CoV-2 spike protein. *Nat Med* **26**, 1422-1427, doi:10.1038/s41591-020-0998-x (2020).
34 Seydoux, E. *et al.* Analysis of a SARS-CoV-2-Infected Individual Reveals Development of Potent Neutralizing Antibodies with Limited Somatic Mutation. *Immunity* **53**, 98-105 e105, doi:10.1016/j.immuni.2020.06.001 (2020).
35 Kreye, J. *et al.* A Therapeutic Non-self-reactive SARS-CoV-2 Antibody Protects from Lung Pathology in a COVID-19 Hamster Model. *Cell* **183**, 1058-1069 e1019, doi:10.1016/j.cell.2020.09.049 (2020).
36 Scheid, J. F. *et al.* B cell genomics behind cross-neutralization of SARS-CoV-2 variants and SARS-CoV. *Cell* **184**, 3205-3221 e3224, doi:10.1016/j.cell.2021.04.032 (2021).
37 Tortorici, M. A. *et al.* Broad sarbecovirus neutralization by a human monoclonal antibody. *Nature* **597**, 103-108, doi:10.1038/s41586-021-03817-4 (2021).
38 Dong, J. *et al.* Genetic and structural basis for SARS-CoV-2 variant neutralization by a two-antibody cocktail. *Nat Microbiol* **6**, 1233-1244, doi:10.1038/s41564-021-00972-2 (2021).
39 Starr, T. N. *et al.* SARS-CoV-2 RBD antibodies that maximize breadth and resistance to escape. *Nature* **597**, 97-102, doi:10.1038/s41586-021-03807-6 (2021).
40 Martinez, D. R. *et al.* A broadly cross-reactive antibody neutralizes and protects against sarbecovirus challenge in mice. *Sci Transl Med*, eabj7125, doi:10.1126/scitranslmed.abj7125 (2021).
41 Onodera, T. *et al.* A SARS-CoV-2 antibody broadly neutralizes SARS-related coronaviruses and variants by coordinated recognition of a virus-vulnerable site. *Immunity* **54**, 2385-2398 e2310, doi:10.1016/j.immuni.2021.08.025 (2021).
42 Raybould, M. I. J., Kovaltsuk, A., Marks, C. & Deane, C. M. CoV-AbDab: the coronavirus antibody database. *Bioinformatics* **37**, 734-735, doi:10.1093/bioinformatics/btaa739 (2021).
43 Barnes, C. O. *et al.* Structures of Human Antibodies Bound to SARS-CoV-2 Spike Reveal Common Epitopes and Recurrent Features of Antibodies. *Cell* **182**, 828-842 e816, doi:10.1016/j.cell.2020.06.025 (2020).
44 Hansen, J. *et al.* Studies in humanized mice and convalescent humans yield a SARS-CoV-2 antibody cocktail. *Science* **369**, 1010-1014, doi:10.1126/science.abd0827 (2020).
45 Kim, S. I. *et al.* Stereotypic Neutralizing VH Clonotypes Against SARS-CoV-2 RBD in COVID-19 Patients and the Healthy Population. *bioRxiv*, 2020.2006.2026.174557, doi:10.1101/2020.06.26.174557 (2020).
46 Du, S. *et al.* Structurally Resolved SARS-CoV-2 Antibody Shows High Efficacy in Severely Infected Hamsters and Provides a Potent Cocktail Pairing Strategy. *Cell* **183**, 1013-1023 e1013, doi:10.1016/j.cell.2020.09.035 (2020).

47 Du, S. *et al.* Structures of SARS-CoV-2 B.1.351 neutralizing antibodies provide insights into cocktail design against concerning variants. *Cell Res* **31**, 1130-1133, doi:10.1038/s41422-021-00555-0 (2021).
48 Harvey, W. T. *et al.* SARS-CoV-2 variants, spike mutations and immune escape. *Nat Rev Microbiol* **19**, 409-424, doi:10.1038/s41579-021-00573-0 (2021).
49 Jones, B. E. *et al.* The neutralizing antibody, LY-CoV555, protects against SARS-CoV-2 infection in nonhuman primates. *Sci Transl Med* **13**, doi:10.1126/scitranslmed.abf1906 (2021).
50 Kemp, S. A. *et al.* SARS-CoV-2 evolution during treatment of chronic infection. *Nature* **592**, 277-282, doi:10.1038/s41586-021-03291-y (2021).
51 Saito, A. *et al.* Enhanced fusogenicity and pathogenicity of SARS-CoV-2 Delta P681R mutation. *Nature*, doi:10.1038/s41586-021-04266-9 (2021).
52 Tan, C. W. *et al.* Pan-Sarbecovirus Neutralizing Antibodies in BNT162b2-Immunized SARS-CoV-1 Survivors. *N Engl J Med* **385**, 1401-1406, doi:10.1056/NEJMoa2108453 (2021).
53 Ehrenmann, F., Kaas, Q. & Lefranc, M. P. IMGT/3Dstructure-DB and IMGT/DomainGapAlign: a database and a tool for immunoglobulins or antibodies, T cell receptors, MHC, IgSF and MhcSF. *Nucleic Acids Res* **38**, D301-307, doi:10.1093/nar/gkp946 (2010).
54 Ehrenmann, F. & Lefranc, M. P. IMGT/DomainGapAlign: IMGT standardized analysis of amino acid sequences of variable, constant, and groove domains (IG, TR, MH, IgSF, MhSF). *Cold Spring Harb Protoc* **2011**, 737-749, doi:10.1101/pdb.prot5636 (2011).
55 Gietz, R. D. & Schiestl, R. H. High-efficiency yeast transformation using the LiAc/SS carrier DNA/PEG method. *Nat Protoc* **2**, 31-34, doi:10.1038/nprot.2007.13 (2007).

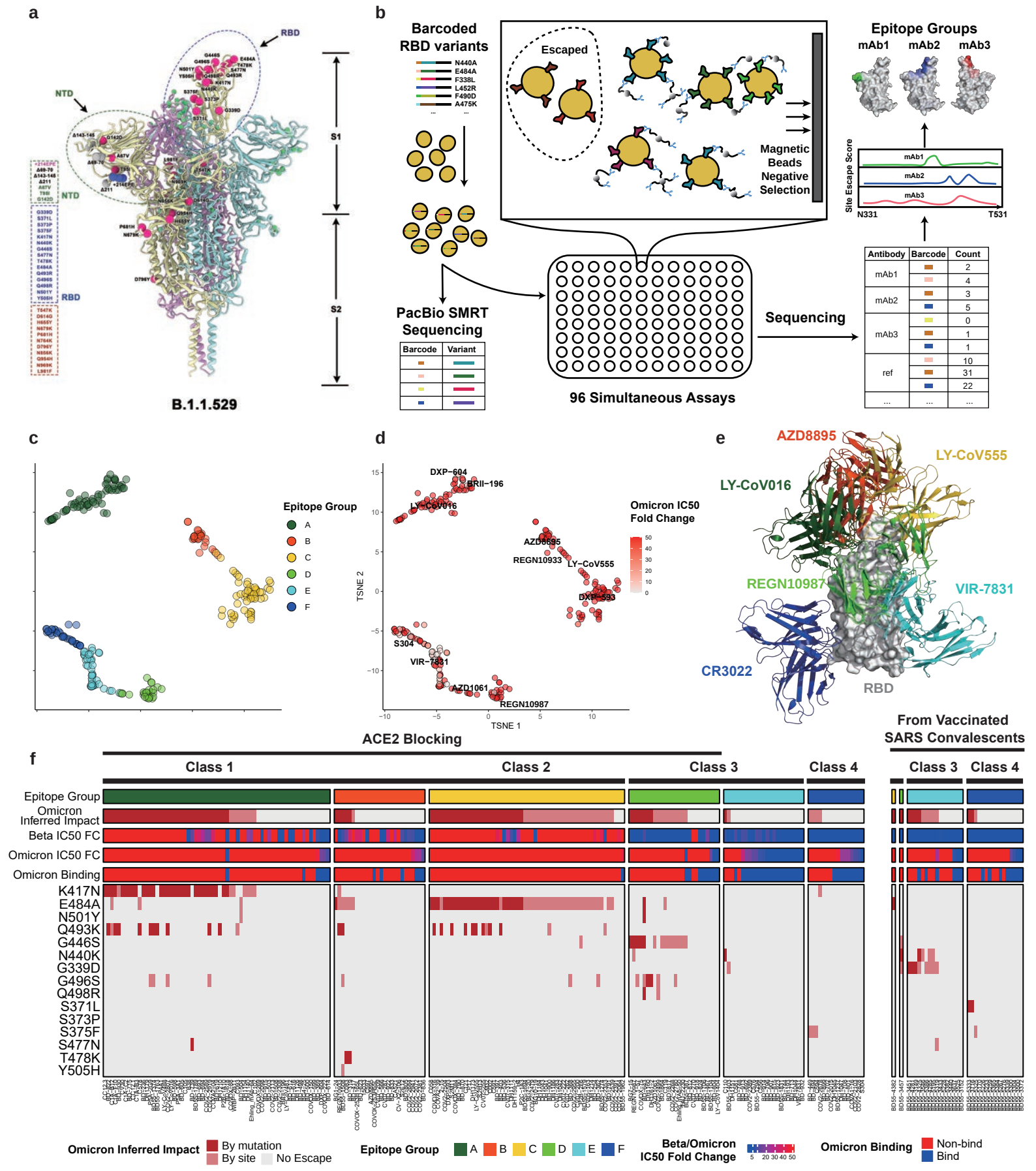

Figure 1. High-throughput escaping mutation screening enables unsupervised NAb clustering and SARS-CoV-2 variant impact inferring.

a) Illustration of B.1.1.529's mutation location on the spike protein. **b)** Schematic of MACS-based high-throughput yeast display mutation screening. **c)** t-SNE embedding and unsupervised clustering of SARS-CoV-2 human NAbs based on each antibody escaping mutation profile. A total of 6 epitope groups (Group A-F) could be defined. **d)** B.1.1.529 pseudovirus neutralizing IC50 of each NAb. **e)** Representative NAb structures of each epitope group. **f)** The impact of each RBD mutation of B.1.1.529 on NAbs' binding. Each NAb's binding to B.1.1.529 RBD was validated through ELISA and BLI.

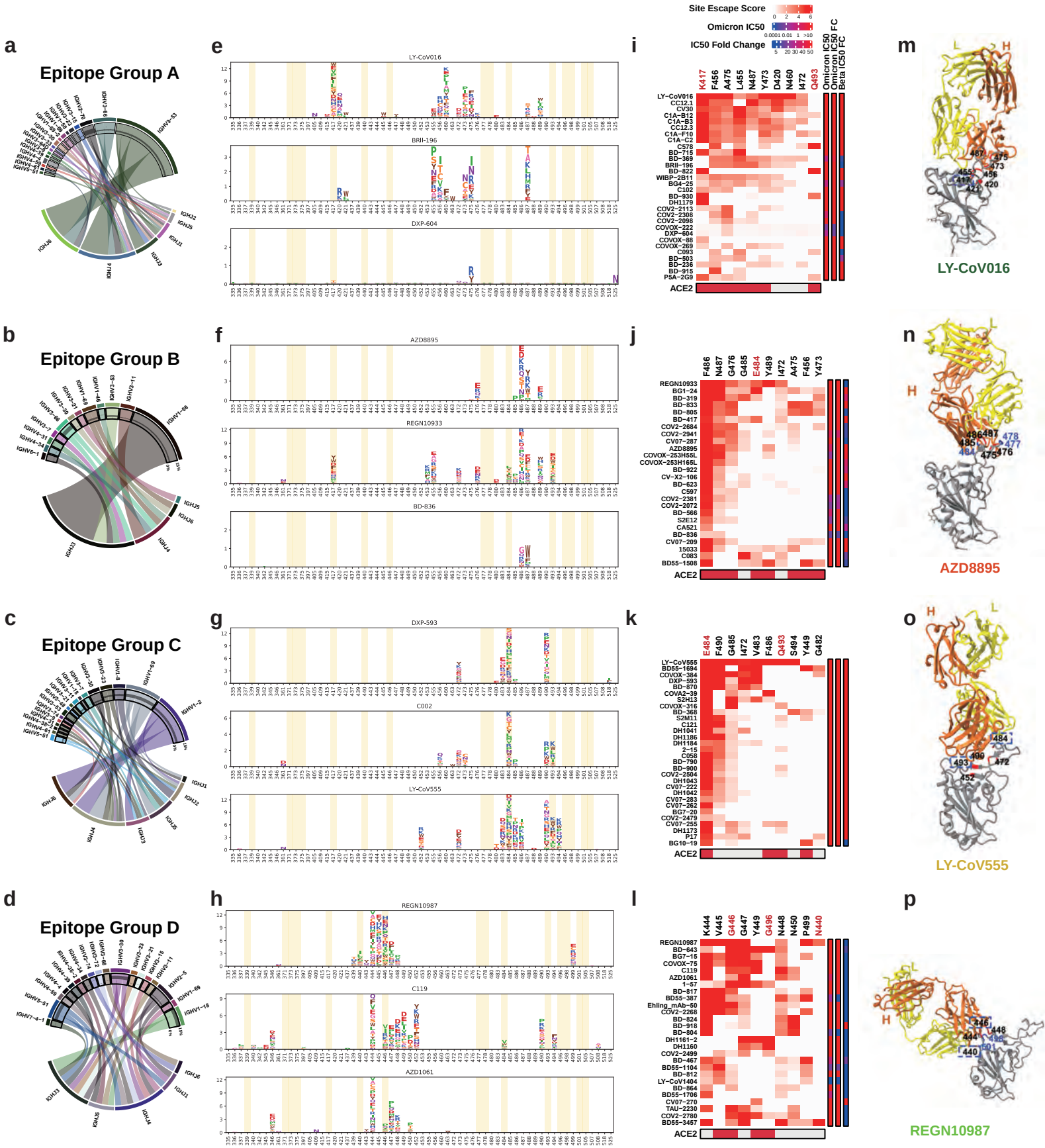

Figure 2. VDJ combination, escape maps, mutations of significant impact, and typical structures in complex with RBD for antibodies of epitope group A-D.

a-d VDJ combination of antibodies' heavy chain variable region and their mutation rate for group A-D, respectively. For each group, the upper semicircle represents IGHV gene distribution and the lower semicircles represent IGHJ gene distribution.

e-h Escape maps of represetative RBD NAbs for group A-D respectively. For each site, the height of a letter indicates the detected mutation escape score of its corresponding residue. Site mutated in Omicron (B.1.1.529) are highlighted.

i-l Heatmaps of site escape scores for RBD NAbs of epitope group A-D, respectively. ACE2 interface residues are annotated with red blocks, and mutated sites in Omicron are marked red. Annotates on the right side of heatmaps represent pseudovirus neutralizing IC50 fold change for Omicron and Beta in comparison with D614G.

m-p Typical structures in complex with RBD of group A-D antibodies. Residues involved in important contacts or related to Omicron mutations are marked.

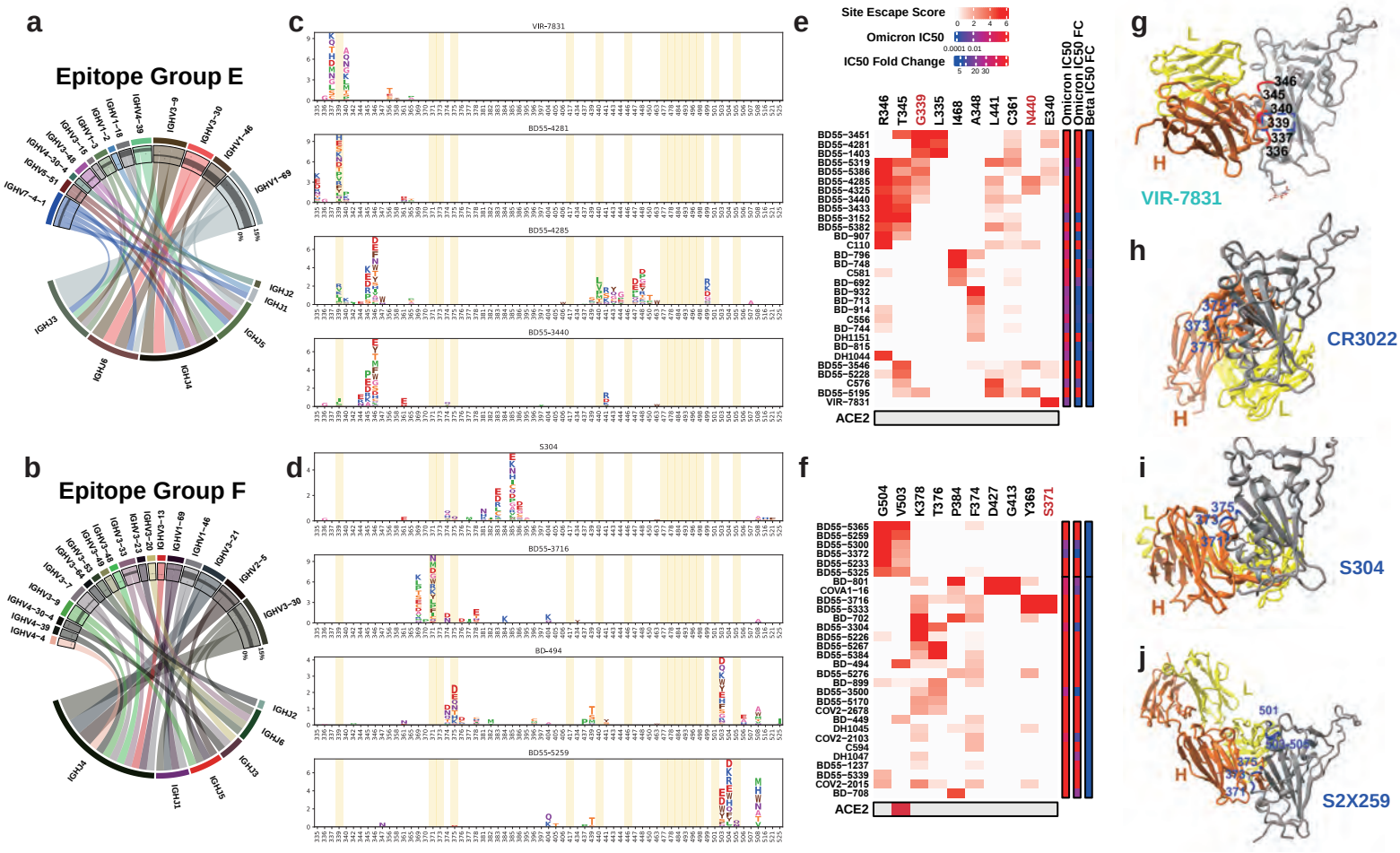

Figure 3. VDJ combination, escape maps, mutations of significant impact, and typical structures in complex with RBD for antibodies of epitope group E-F.

a-b VDJ combination of antibodies' heavy chain variable region and their mutation rate for group E-F, respectively. For each group, the upper semicircle represents IGHV gene distribution and the lower semicircles represent IGHJ gene distribution.

c-d Escape maps of represetative RBD NAbs for group E-F respectively. For each site, the height of a letter indicates the detected mutation escape score of its corresponding residue. Site mutated in Omicron (B.1.1.529) are highlighted.

e-f Heatmaps of site escape scores for RBD NAbs of epitope group E-F, respectively. ACE2 interface residues are annotated with red blocks, and mutated sites in Omicron are marked red. Annotates on the right side of heatmaps represent pseudovirus neutralizing IC50 fold change for Omicron and Beta in comparison with D614G.

g-j Typical structures in complex with RBD of group E-F antibodies. Residues involved in important contacts or related to Omicron mutations are marked.

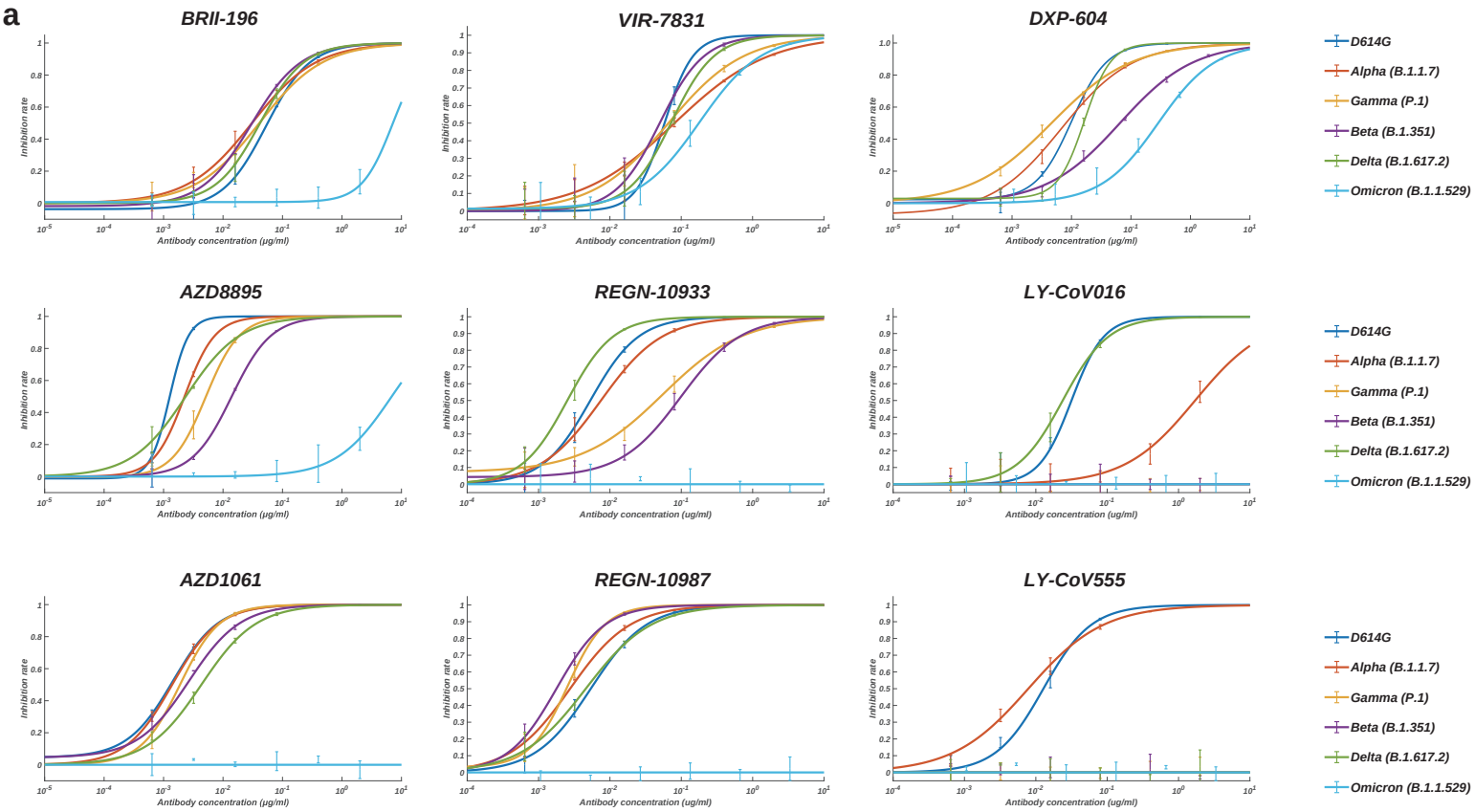

b

	D614G	Alpha	Gamma	Beta	Delta	Omicron
LY−CoV555	0.013	0.008	>10	>10	>10	>10
LY−CoV016	0.032	1.707	>10	>10	0.024	>10
REGN10933	0.005	0.007	0.055	0.098	0.003	>10
REGN10987	0.005	0.003	0.003	0.002	0.005	>10
AZD8895	0.001	0.002	0.012	0.014	0.002	6.860
AZD1061	0.001	0.001	0.002	0.003	0.004	>10
VIR−7831	0.058	0.080	0.066	0.050	0.073	0.181
BRII−196	0.053	0.031	0.041	0.030	0.042	7.258
DXP−604	0.010	0.007	0.005	0.065	0.016	0.287

IC50 (ng/μL)
0 5 10

c

	Antibody	BD55-3152	BD55-5319	BD55-5386	BD55-5300	BD55-3372	BD55-3500
	Epitope Group	E	E	E	F	F	F
Variants Pseudovirus IC50 (μg/mL)	D614G	0.0105	0.0150	0.0005	0.0051	0.0068	0.1053
	Beta	0.0076	0.0040	0.0011	0.0031	0.0073	0.2326
	Omicron	0.0142	0.3685	0.0584	0.0663	0.0097	0.2610
Sarbecovirus RBD ELISA (OD450)	SARS-CoV-1	3.462	3.447	3.417	3.405	3.467	3.476
Clade 1b	RaTG13	0.353	0.135	0.086	0.193	0.061	3.258
	Pangolin-GD	1.132	2.657	0.421	3.526	3.493	3.57
	Pangolin-GX	0.996	0.812	1.95	0.709	2.889	3.403
Clade 1a	SARS-CoV-1 PC4-127	3.598	3.523	3.473	3.531	3.557	3.457
	SARS-CoV-1 Sin852	3.458	3.495	3.468	3.464	3.413	2.984
	WIV1	2.409	1.976	3.336	3.588	3.515	3.603
Clade 3	BM48-31	0.133	3.424	0.115	3.483	3.515	3.476
Clade 2	YN2013	0.168	0.244	0.074	0.601	0.072	2.683

Fig. 4 Pseudovirus neutralization and RBD binding affinity of various SARS-CoV-2 NAbs. **a**, Neutralization of SARS-CoV-2 variants of concern (pseudotyped VSV) by 9 clinical antibody drugs. Data are collected from three technical replicates, and error bars show mean±s.d. **b**, IC50 values calculated from data in Fig. 4a. **c**, SARS-CoV-2 variants pseudovirus IC50 and sarbecovirus RBD binding affinity (mea-sured by ELISA OD450) of selected potent Omicron-neutralizing antibodies.

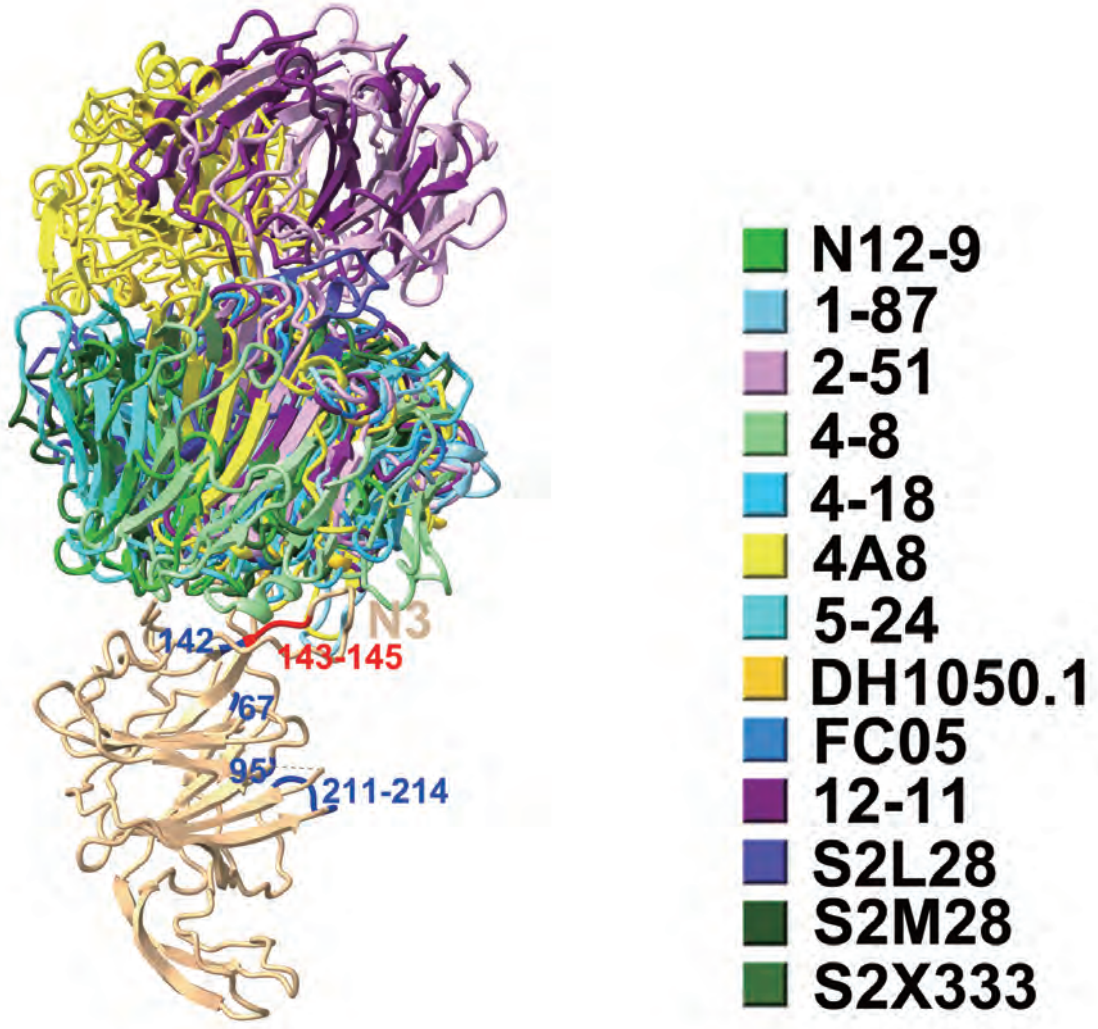

Extended Data Fig. 1 Structures of SARS-CoV-2 NTD-binding neutralizing antibodies.
NTD-binding NAbs are shown together in different colors in complex with one NTD, and most of them contact with residues 142-145, which indicates their high probability to be escaped by G142D and Δ 143-145 of Omicron. Missense mutations and deletions of Omicron NTD are colored blue and red, respectively.

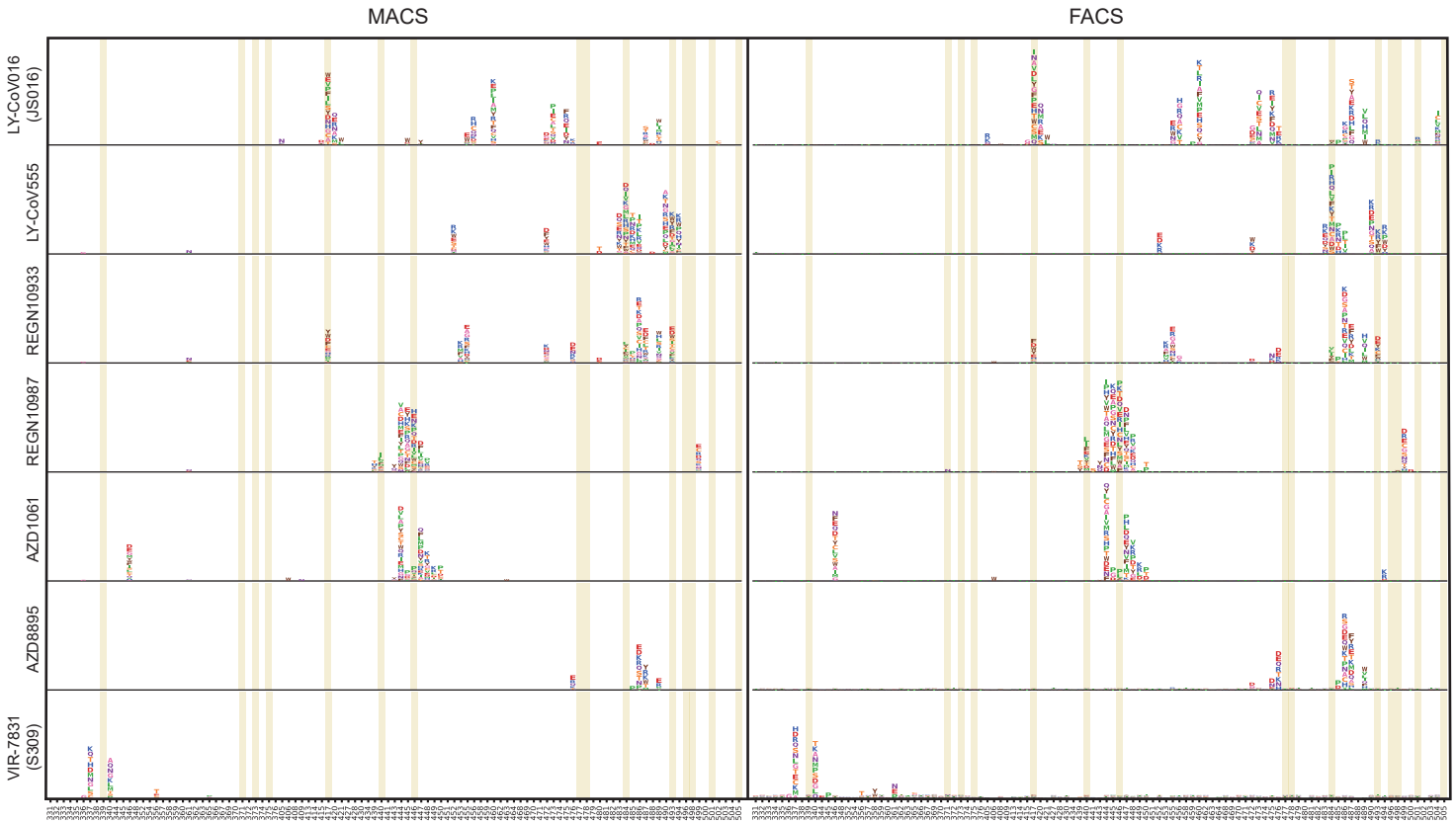

Extended Data Fig. 2 Comparison between FACS and MACS-based deep mutational scanning for epitope identification of SARS-CoV-2 RBD antibodies.
Deep mutational scanning maps with MACS-based (left) and FACS-based assays (right) of therapeutic neutralizing antibodies that have received emergency use authorization from the US FDA. Sites mutated in Omicron variant are highlighted.

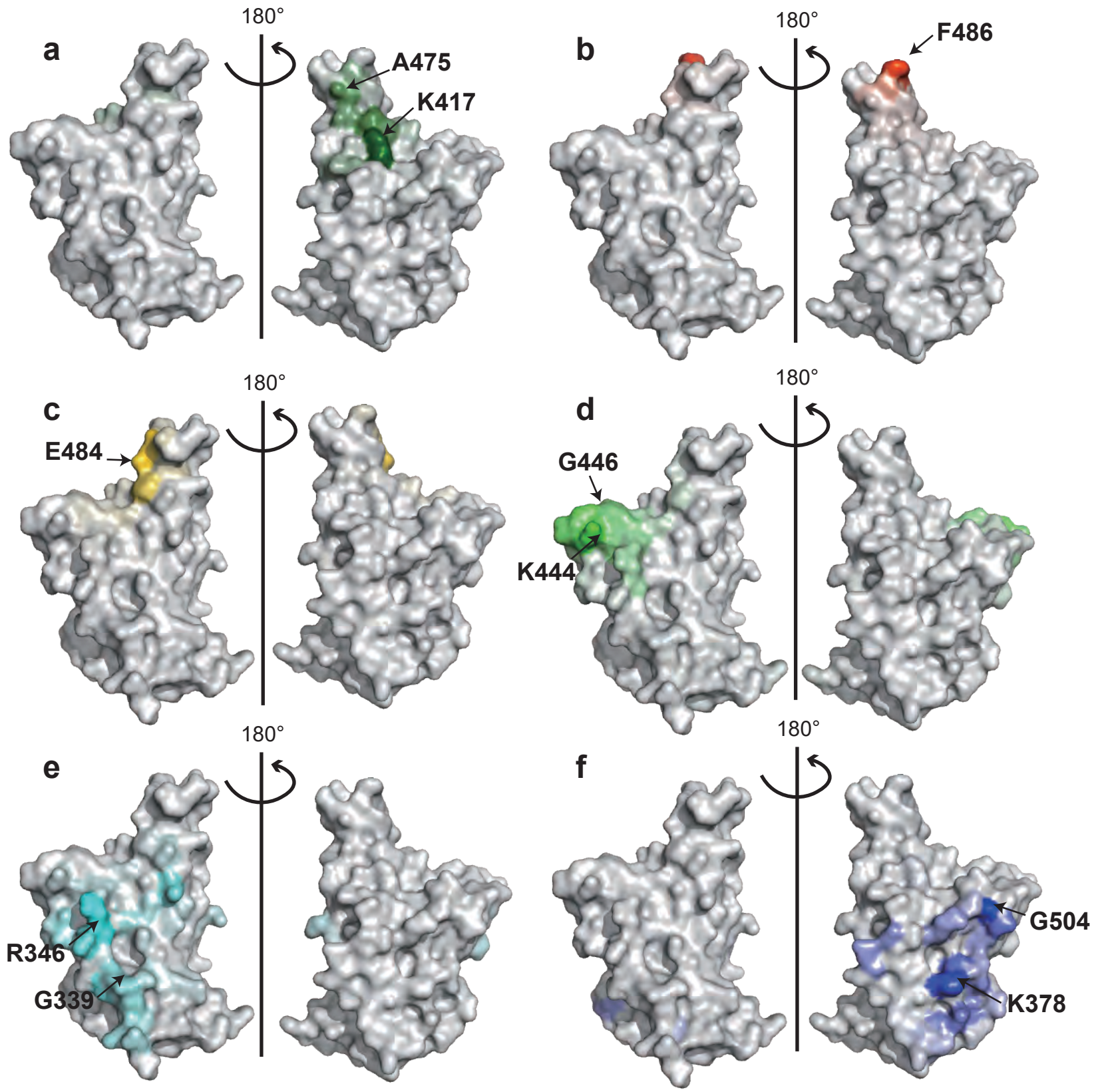

Extended Data Fig. 3 SARS-CoV-2 RBD antibodies of different epitope groups show distinct escape hotspots on RBD surface.
(a)-(f) correspond to aggregated site escape scores of epitope group A-F, respectively. Escape hotspots of each epitope group are annotated by arrows.

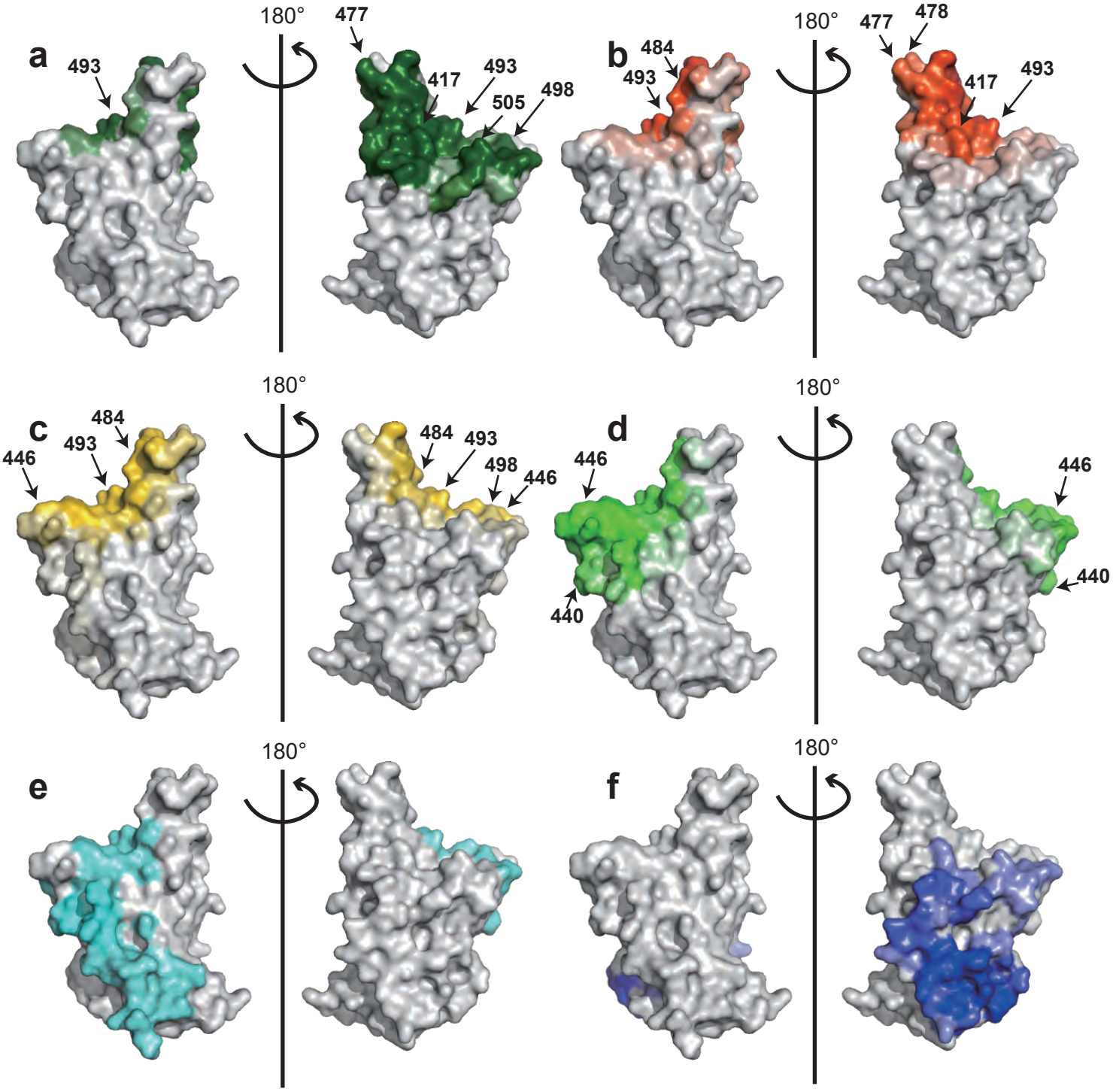

Extended Data Fig. 4 SARS-CoV-2 RBD antibodies of different epitope groups show distinct spatial contact footprints on RBD surface.
(a)-(f) correspond to aggregated footprints of epitope group A-F, respectively. Publicly availble structures of neutralizing antibodies in complex with SARS-CoV-2 RBD are gathered from PDB and classified into groups. Different colors distinguish epitope groups, and the darkness reflects group-specific site popularity to appear on the complex interface. Common interface residues of each group are marked by arrows.

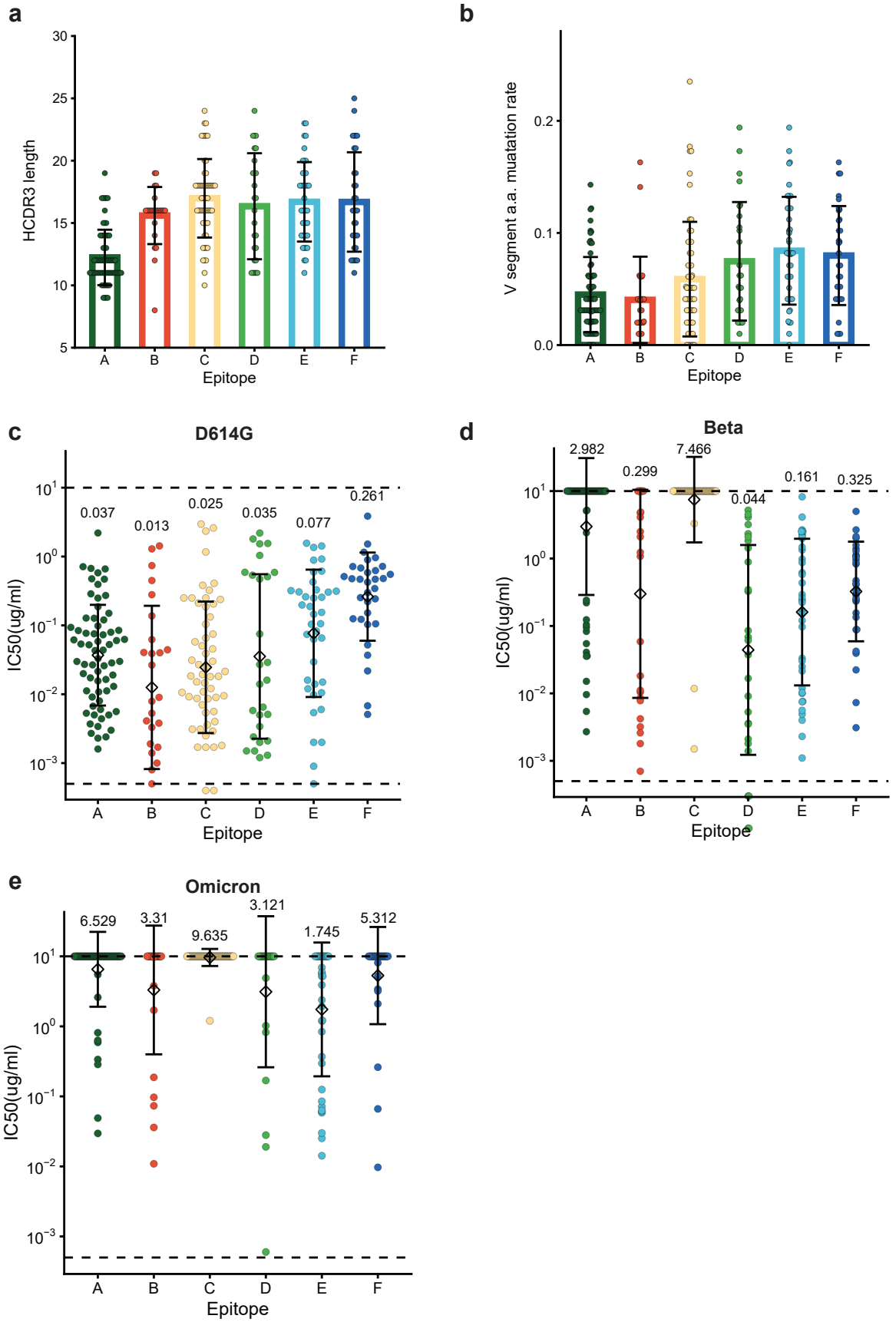

Extended Data Fig. 5. Antibody features and pseudovirus neutralizing IC50s.

a) The length of H chain complementarity-determining region 3(HCDR3) amino acid sequence. Scatters show the individual HCDR3 length of antibody, vertical bars show the mean value, and error bars show mean ± sd. **b)** The V segment amino acid(a.a.) mutation rate. Mutation count divided by the a.a. length of V segment is defined as the mutation rate of V segment. Scatters show the individual H chain V segment mutation rate of antibody, vertical bars show the mean value, and error bars show mean ± sd.
c-e) IC50 of antibodies in the D614G(**c**), Beta(**d**), and Omicron(**e**) mutant pseudovirus neutralizing assay. Scatters show the individual IC50 of antibody, diamonds show the IC50 geometric mean(GM) of each epitope, and error bars show GM ± sd in the log10 scale. Dotted lines show the limit of detection, which is from 0.0005 ug/ml to 10 ug/ml. IC50 GMs are also noted on the figure.

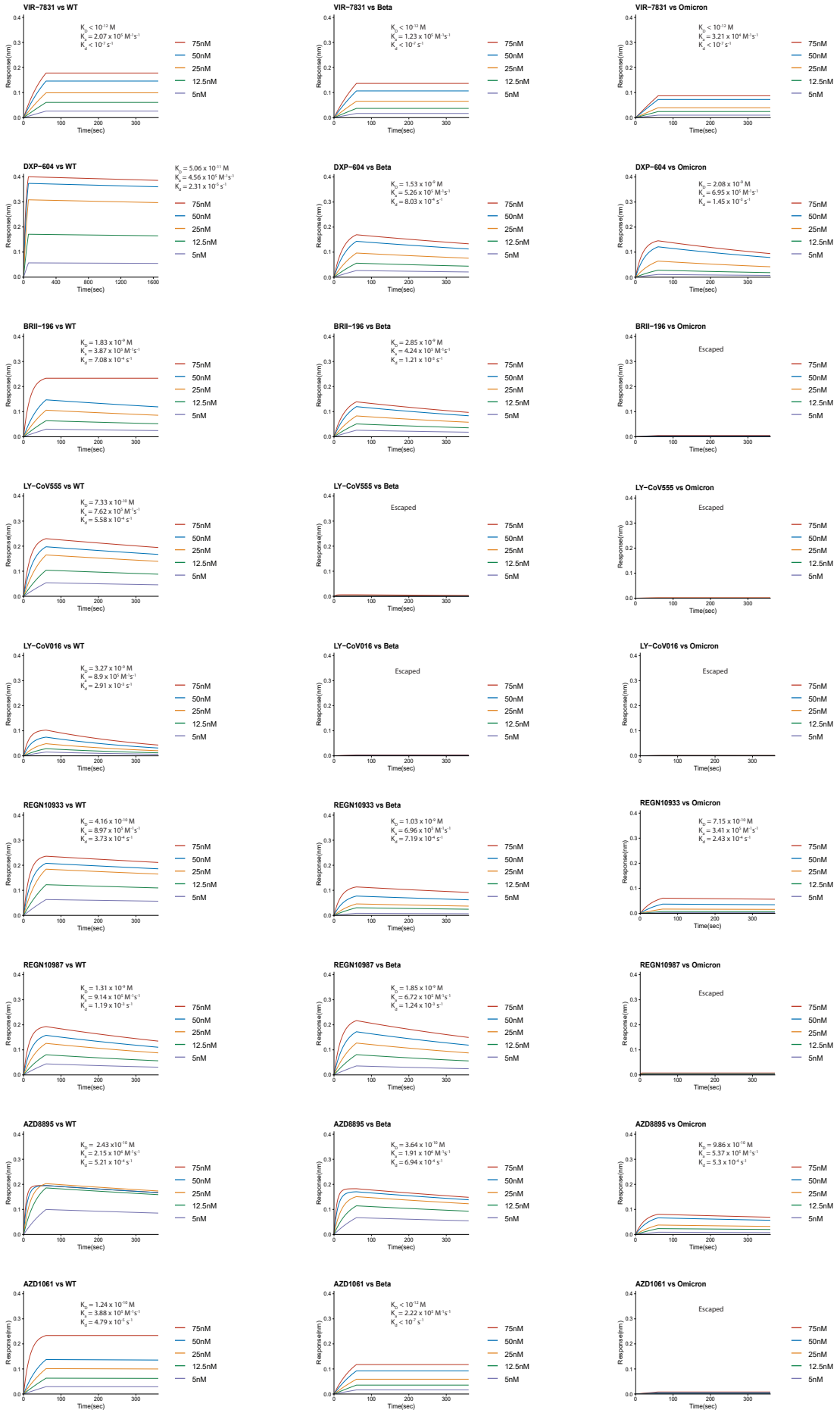

Extended Data Fig. 6. Fitted line plot showing the BLI response between antibodies and the receptor binding domain(RBD) of SARS-CoV-2 WT, Beta, or Omicron strain.
The concentrations of RBD are shown in different colors. Dissociation constant(KD), associationconstant(Ka) and dissociation rate constant(Kd) are noted on the figure. The assays without binding are marked as “Escaped”.

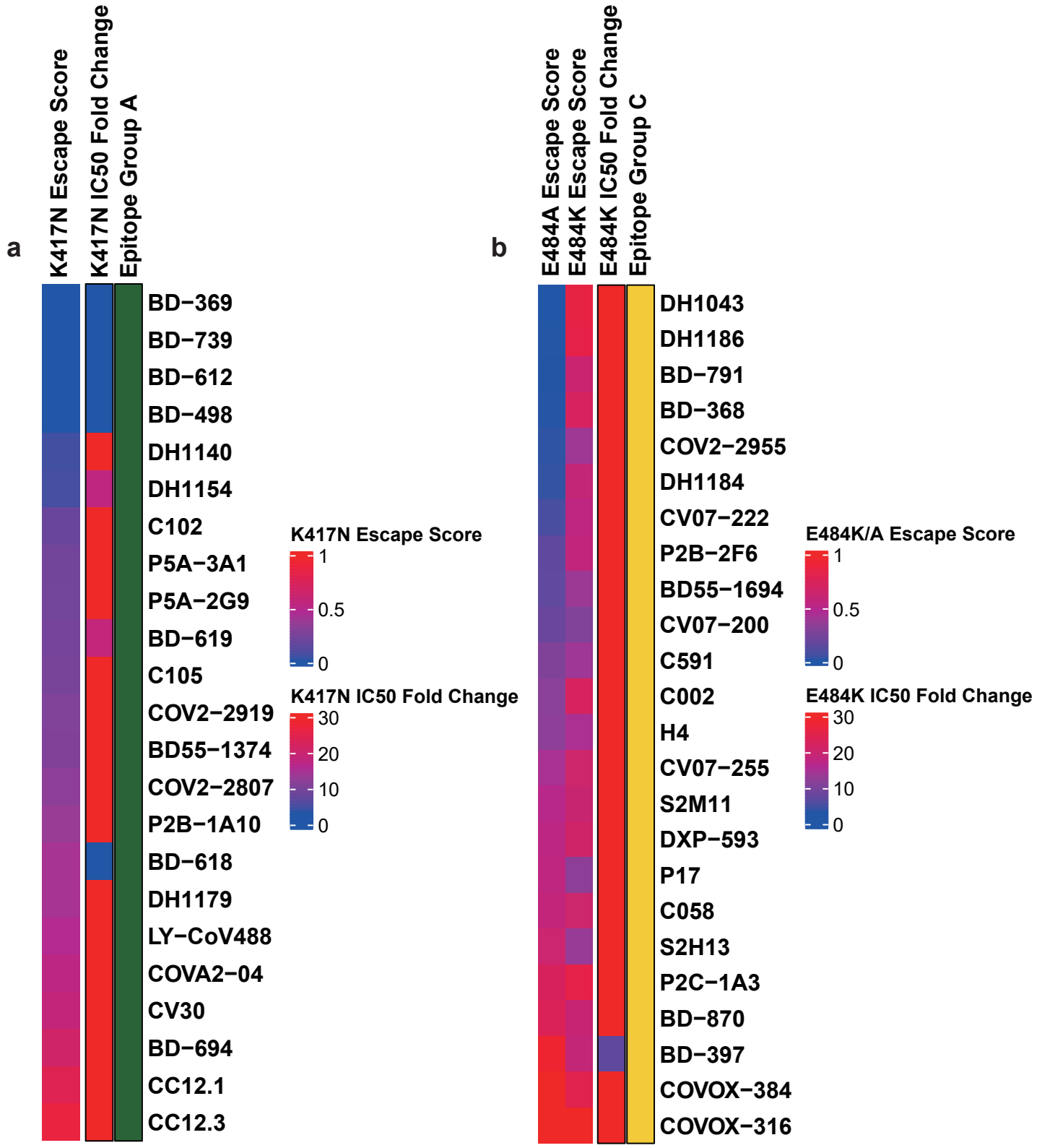

Extended Data Fig. 7 Comparison between mutation escape scores estimated from high throughput deep mutational scanning and neutralization IC50 of pseudovirus with corresponding mutations.
(a) K417N escape scores and corresponding K417N pseudovirus neutralizing IC50 fold change compared to D614G pseudovirus of antibodies within epitope group A.
(b) E484K/E484A escape scores and corresponding E484K pseudovirus neutralizing IC50 fold change compared to D614G pseudovirus of antibodies within epitope group C.